HAL
open science

Anisotropic and low damage III-V/Ge heterostructure etching for multijunction solar cell fabrication with passivated sidewalls

Mathieu de Lafontaine, Erwine Pargon, Camille Petit-Etienne, Sylvain David, Jean-Paul Barnes, Névine Rochat, Abdelatif Jaouad, Maïté Volatier, Simon Fafard, Vincent Aimez, et al.

To cite this version:

Mathieu de Lafontaine, Erwine Pargon, Camille Petit-Etienne, Sylvain David, Jean-Paul Barnes, et al.. Anisotropic and low damage III-V/Ge heterostructure etching for multijunction solar cell fabrication with passivated sidewalls. Micro and Nano Engineering, 2021, pp.100083. 10.1016/j.mne.2021.100083 . hal-03171055

HAL Id: hal-03171055

https://hal.science/hal-03171055

Submitted on 6 Oct 2021

HAL is a multi-disciplinary open access archive for the deposit and dissemination of scientific research documents, whether they are published or not. The documents may come from teaching and research institutions in France or abroad, or from public or private research centers.

L'archive ouverte pluridisciplinaire **HAL**, est destinée au dépôt et à la diffusion de documents scientifiques de niveau recherche, publiés ou non, émanant des établissements d'enseignement et de recherche français ou étrangers, des laboratoires publics ou privés.

MNE 11 (2021) 100083

Contents lists available at ScienceDirect

Micro and Nano Engineering

journal homepage: www.sciencedirect.com/journal/micro-and-nano-engineering

Research paper

Anisotropic and low damage III-V/Ge heterostructure etching for multijunction solar cell fabrication with passivated sidewalls

Mathieu de Lafontaine [a,b,*], Erwine Pargon [a], Guillaume Gay [a], Camille Petit-Etienne [a], Sylvain David [a], Jean-Paul Barnes [c], Névine Rochat [c], Abdelatif Jaouad [b], Maïté Volatier [b], Simon Fafard [b], Vincent Aimez [b], Maxime Darnon [b]

[a] Univ. Grenoble Alpes, CNRS, CEA/LETI-Minatec, Grenoble INP, LTM, F-38054 Grenoble, France
[b] Laboratoire Nanotechnologies Nanosystèmes (LN2) – CNRS IRL-3463 Institut Interdisciplinaire d'Innovation Technologique (3IT), Université de Sherbrooke, 3000 Boulevard Université, Sherbrooke, J1K OA5, Québec, Canada
[c] Univ. Grenoble Alpes, CEA, Leti, F-38000 Grenoble, France

ARTICLE INFO

Keywords:
Plasma etching
III-V semiconductors
$SiCl_4/H_2$ plasma
Through cell via contacts
Multijunction solar cells
Concentrated photovoltaics

ABSTRACT

This article presents a complete plasma etching process to etch high aspect ratio patterns on III-V/Ge solar cell heterostructure with low damage for the fabrication of multijunction solar cells with a through cell via contact architecture. A $SiCl_4/H_2$ chemistry was studied with different hydrogen dilutions within the plasma (0%, up to 67%) and with different cathode temperatures (20°C, up to 200°C). This chemistry choice creates a $SiCl_x$-based inhibiting layer on the sidewalls that promotes anisotropic etching through the epitaxial heterostructure. The study suggests that a high hydrogen flow and a low temperature reduce the chemical reactions that create sidewall erosion. A high hydrogen flow appears to provide a hydrogen passivation of the non-radiative defects on the III-V heterostructure sidewall during the etching process. III-V/Ge triple junction solar cells with standard grid line and busbar front and back contacts have been fabricated and via-holes were plasma-etched through the active layers in order to investigate the impact of hydrogen passivation on the photovoltaic performance. The results demonstrate that the hydrogen passivation enables an open-circuit voltage increase that persists even after 5 months. This plasma process can also be used for the mesa etching step on multijunction solar cells with standard contacts. Thus, it could provide an appealing pathway to increase the conversion efficiency of state-of-the-art multijunction solar cells with standard contacts. To complete the etching process, a liner is used to protect the sidewall properties and a time-multiplexed Ge etching process is proposed to finalize the patterning and even open a pathway towards III-V/Ge plasma dicing.

1. Introduction

Over the past few years, through cell via contacts for multijunction solar cells have been the object of a growing interest to replace standard grid line and busbar front contact. [23,28,31,33,34,37] A schematic of the new contact architecture is presented in Fig. 1. [11] The goal of this new interconnection design is to reduce the shading and the resistive losses by transferring the front side contact towards the backside by using electrically insulated and metallized vias. [33] From simulation results, an absolute cell efficiency increase of 3% could be expected by using through cell via contact instead of standard contacts. [33] The busbar suppression could also increase the power yield per wafer by 20%. [33] Another study has shown that this architecture could reduce the losses from the light non-uniformities. [31] Finally, this new architecture has been successfully fabricated on InGaP/AlGaAs dual junction heterostructure. [28,34] To the best of our knowledge, through cell via contacts were never fabricated on III-V/Ge triple junction heterostructures.

Plasma etching anisotropic via-holes with low sidewall damage and high aspect ratio (AR) still represents a challenge in fabricating through cell via contacts on III-V/Ge triple junction heterostructures. Indeed, an heterostructure consisting of several III-V layers (InGaP, (In)GaAs, GaAs, AlInP, AlGaInP, AlGaAs) and quantum dot materials grown on germanium must be etched with a high aspect ratio (AR>3), a good anisotropy and with limited sidewall damage. Only a few studies have been published on multijunction solar cells plasma etching and different plasma

* Corresponding author.
E-mail address: mathieu.de.lafontaine@usherbrooke.ca (M. de Lafontaine).

https://doi.org/10.1016/j.mne.2021.100083
Received 22 December 2020; Received in revised form 10 February 2021; Accepted 1 March 2021
Available online 13 March 2021
2590-0072/© 2021 The Authors. Published by Elsevier B.V. This is an open access article under the CC BY license (http://creativecommons.org/licenses/by/4.0/).

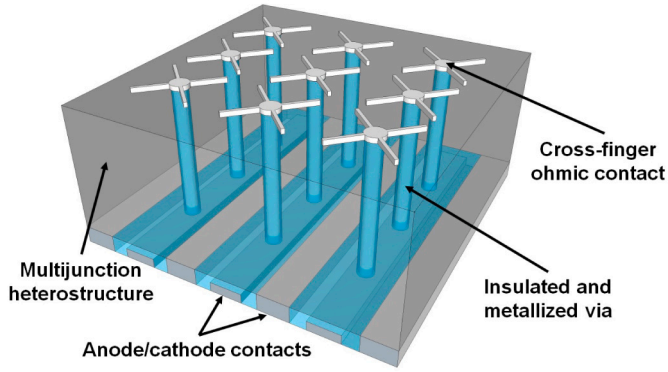

Fig. 1. Schematic of a multijunction solar cell with a through cell via contact architecture. [11].

chemistries were used. Cl_2/Ar and BCl_3/Cl_2 have been used to etch shallow vias (AR⩽1). [10,37] However, these chemistries might not be suited to perform high aspect ratio anisotropic etching since a chlorine-rich chemistry may generate significant sidewall erosion. [11] It was previously shown that using $SiCl_4$-based plasma can reduce the sidewall erosion thanks to the $SiCl_x$ inhibiting layer. [11,38] Furthermore, hydrogen addition to the plasma chemistry further reduces the sidewall erosion. [11] In addition, hydrogen plasma has also been used previously for its passivating properties. [24,35,36] Finally, we have shown that a time-multiplexed plasma process may be used for anisotropic Ge etching with a high aspect ratio. [9].

Solar cell performance is expected to be lowered after plasma etching due to surface recombination on the sidewall by a larger perimeter-to-area ratio. [2,10,14] Furthermore, it is possible that the process creates plasma-induced damage on the sidewalls. [11] It was demonstrated that by choosing the proper plasma chemistry, it may be possible to reduce the plasma damage and the associated photovoltaic performance loss. [11] Plasma damage on the etched sidewall must therefore be characterized and limited.

In this study, a complete plasma etching process is proposed and characterized to pattern high aspect ratio via-holes on III-V/Ge multijunction heterostructures. The etch morphology was characterized by scanning electron microscopy (SEM) and scanning transmission electron microscopy (STEM). The chemical composition of the etched sidewall was analyzed by energy-dispersive spectroscopy (EDX) and time-of-flight secondary ion mass spectrometry (ToF-SIMS). Cathodoluminescence measurements were also performed in order to evaluate the plasma damage on the sidewalls. Furthermore, multijunction solar cells with standard contacts and via-holes etched with this process have been fabricated in order to evaluate the possible photovoltaic performance loss induced by the plasma process.

2. Experiments

2.1. Etching process

The epiwafers used in this study are quantum dot-enhanced III-V/Ge triple junction heterostructures that consist of an In-rich (~25%) InGaP top cell, an (In)GaAs middle cell (with low In content ~1%) and a Ge bottom cell. [15] A cross-section scanning electron microscope (SEM) image of the ~7μm-thick III-V epitaxy is presented in Fig. 2.

A complete etching process has been developed to pattern deep (>50μm) and anisotropic vias on III-V/Ge heterostructures and its schematics are outlined in Fig. 3. The first fabrication step consists in patterning a 5μm-thick silicon oxide hard mask on the epitaxial heterostructure (Fig. 3 a). Silicon oxide is deposited by plasma-enhanced chemical vapor deposition (PECVD). It is then patterned by using contact photolithography and a $Ar/C_4F_8/O_2$ magnetically-enhanced

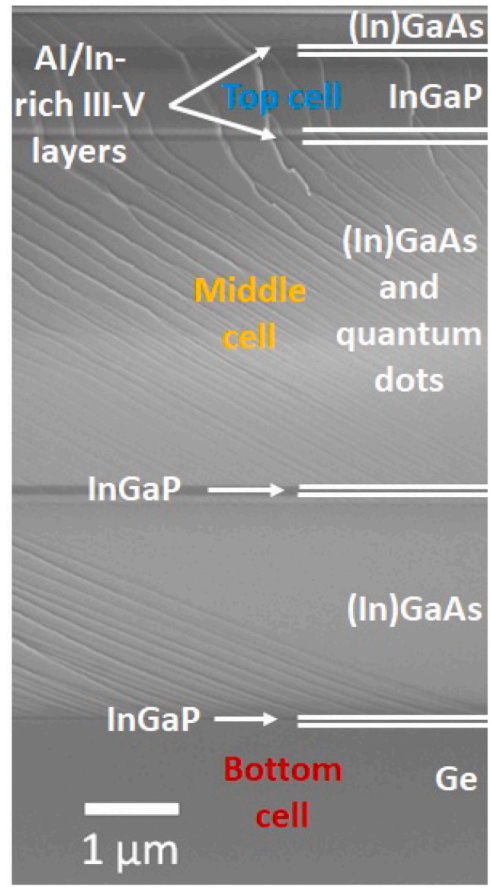

Fig. 2. Cross-section scanning electron image of the III-V/Ge triple junction heterostructure.

reactive ion etching plasma process (MERIE). The patterns consist in via-holes with a diameter of 5μm, up to 50μm and trenches with a width of 5μm, up to 100μm. These patterns will lead to an aspect ratio ranging between 0.7 and 8 after the complete etching process. Then the active region of the III-V/Ge heterostructure is etched as presented in Fig. 3 b. The plasma etching experiments are carried out in an inductively coupled plasma (ICP) reactor, the Plasmalab100 ICP etcher from Oxford. Both the bias power and the inductive source power are operated at 13.56 MHz. The 1 cm × 1 cm samples were mounted on a 4″ silicon wafer covered with silicon oxide deposited by PECVD. Fomblin oil was used to ensure a good thermal conductivity between the sample and the carrier wafer. The main etching gas used was $SiCl_4$, to which, hydrogen could be added as a secondary gas with different ratio to the total gas flow (0%, 33% or 67%). The etching experiments were performed at three different temperatures: 20°C, 140°C and 200°C. The total gas flow was set to 18sccm and the pressure was controlled at 4mTorr. The inductive source and bias power were set to 440 W and 260 W respectively for the results presented in Sections 3.1.1, 3.1.2 and 3.1.3. Unfortunately, due to a chamber condition drift, the inductive source and bias power had to be updated to 550 W and 470 W respectively for the results presented in Sections 3.1.4, 3.1.5 and 3.2. This update had to be made to keep the same etch morphology (for each condition sets) throughout the study. After this first etching step, the active region sidewalls are protected from further damage with a ~100nm-thick silicon oxide liner deposited by PECVD, as shown in Fig. 3 c. The liner is etched at the bottom of the patterns (Fig. 3 d) with an anisotropic CF_4 plasma in the same Oxford ICP reactor. Then, the via etching is completed by using a time-multiplexed plasma etching process to etch the Ge substrate, as presented in Fig. 3 e. The hard mask and the silicon oxide liner can then be removed by using a 49% hydrofluoric acid

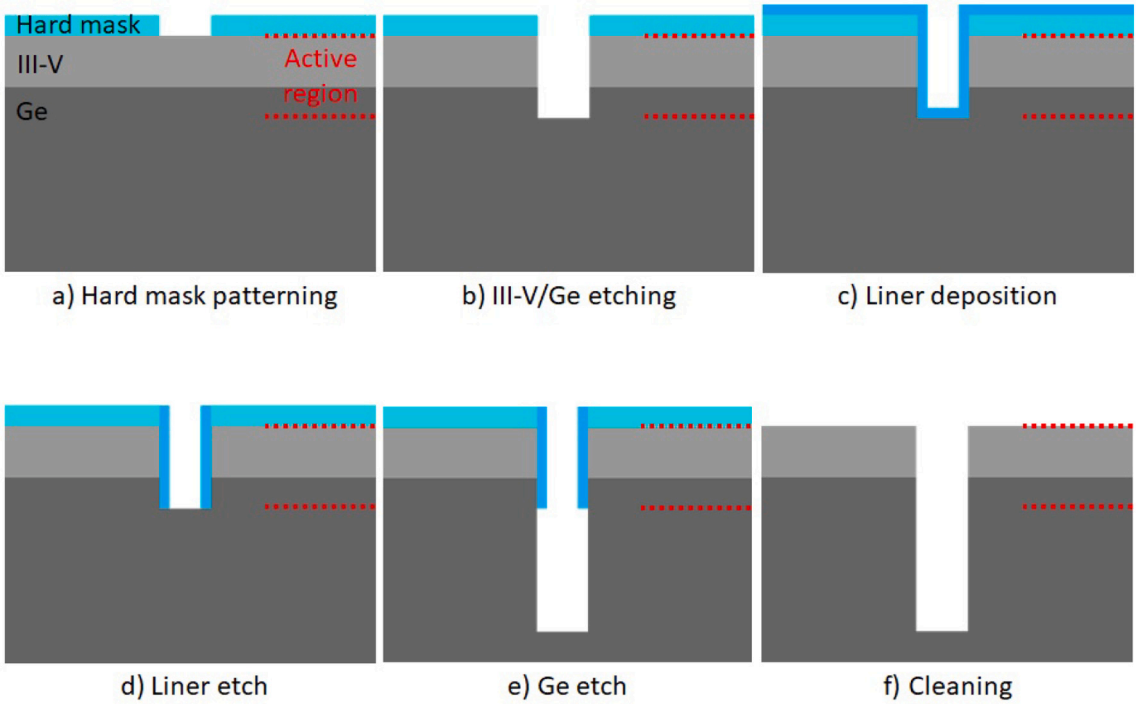

Fig. 3. Schematics of the complete via-hole etching process.

immersion for 5 min. (Fig. 3 f).

2.2. Etching process characterization

After the first etching step (Fig. 3 b), several characterizations were performed. The samples were cleaved in order to study the etched sidewalls. The etch morphology was characterized by scanning electron microscopy (SEM) and scanning transmission electron microscopy (STEM). For samples with severe erosion over all the layers, the hard mask was used as a reference to extract the sidewall erosion values. After etching, the chemical composition of the inhibiting layer was analyzed by energy-dispersive spectroscopy (EDX). The SEM-EDX detector used was an XFlash detector 5030 from Bruker whereas the TEM-EDX detector was from Oxford.

Then, the inhibiting layers are removed with a 1% HF dip selectively over the III-V/Ge sidewalls. After the inhibiting layer removal, the III-V/Ge sidewalls were studied by time-of-flight secondary ion mass spectrometry (ToF-SIMS) and cathodoluminescence. The ToF-SIMS analyses were performed with an Ion-TOF TOF-SIMS5 instrument with a detection of the negative ions only. A Bi_3^{2+} beam at 30 kV was used for the analysis with a 21*21μm field of view, a 70μs cycle time, and a 512 pixels resolution. The sample was tilted to perform the mapping on the etched sidewall of a 100μm-wide trench, as shown in Fig. 4 a). The mass of the ions sputerred from the sample surface is recorded over the experiment duration, allowing to reconstruct an ion profile with the sputtering time. At the end of the process, the pattern depth generated by the sputtering is measured by AFM to convert the time scale into a sputtered depth.

The plasma damage on the sidewalls was also studied by cathodoluminescence. The measurements were performed in a Rosa instrument from Attolight and the samples were cooled with liquid He to 4 K. Fig. 4 b) shows the area probed during the measurements. The samples were cleaved in order to expose the sidewalls of a 50μm diameter via. This large via size was chosen to minimize the possible luminescence contribution from the cleaved sidewall. The via sidewalls were probed on a centered 8*8μm raster. Furthermore, a 3 keV beam energy was chosen to limit the bulk luminescence as the beam only probed the first ~50nm. The cathodoluminescence data are analyzed with the Labspec software that enables to extract the cathodoluminescence coming from the InGaP top cell and the (In)GaAs middle cell only.

2.3. Multijunction solar cell fabrication

Furthermore, the impact of the etching process was also studied on the photovoltaic performance. Multijunction solar cells with standard contacts (busbar and grid line front contact and back contact) were fabricated. Using the aforementioned plasma process (up to step b of Fig. 3), shallow (~10μm) via holes were etched on the solar cells in order to assess the photovoltaic performance loss associated to via-hole etching. The complete solar cell fabrication process is detailed in previous publications. [10] The back contact is formed by a Ni/Au evaporation. The grid line and busbar front contact is patterned by photolithography and Ni/Ge/Au/Ni/Au evaporation. A second photolithography and a plasma etching process detailed above is performed to pattern the 10 μm-diameter vias on the cells and trenches to electrically isolate one cell from another. On those samples, photoresist was used as a mask instead of PECVD SiO_2. One row of vias was patterned between every grid line and the pitch between the vias of a row was 60, 80 or 100μm. The latest characteristic allowed to vary the perimeter-to-area ratio to study the total plasma damage on the device, which scales with the sidewall surface area. Some devices did not have any vias patterned and were used as reference cells in order to assess the plasma damage associated specifically to via-hole etching. Those reference samples also need plasma patterning to electrically isolate the solar cells, meaning that for each plasma chemistries investigated, there is a reference sample. The comparison of the photovoltaic performance of the different reference samples (with no vias) also gives an insight on the plasma chemistry impact, which is especially relevant for solar cell isolation applications. The photovoltaic performance was studied as a function of the hydrogen ratio to the total gas flow during the plasma process. For the solar cell fabrication, the cathode temperature was fixed at 20°C during the plasma process. The last step consists in etching the contact layer in a $NH_4OH/H_2O_2/H_2O$ solution. Despite the fact that these solar cells aim to evaluate the loss associated to via-hole etching

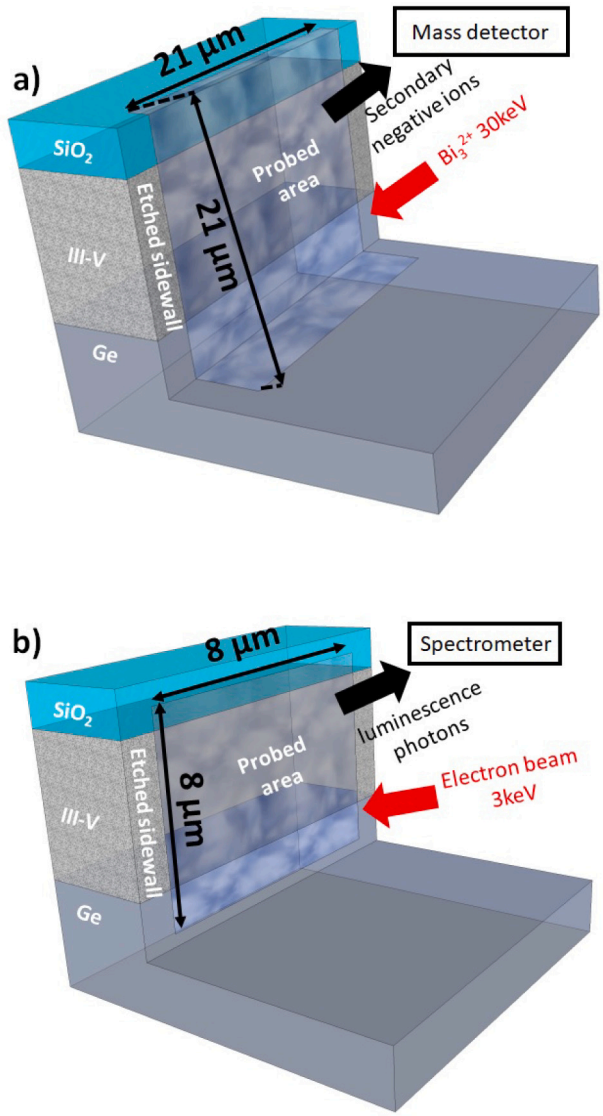

Fig. 4. Schematic of the a) ToF-SIMS measurement setup of the etched sidewall and b) the cathodoluminescence measurement setup of the etched sidewall.

and plasma damage, the (In)GaAs middle cell sidewalls and Ge may be slightly etched during this chemical etching step [11].

2.4. Multijunction solar cell characterization

To assess the plasma damage, the via-hole etching and the impact of hydrogen addition on the solar cell performance, one-sun current-voltage (IV) measurements were performed. The open-circuit voltage (V_{oc}) was specifically studied since it is the parameter that is the most sensitive to the plasma damage on the sidewalls. The Newport Oriel Sol1A solar simulator with an AM1.5D spectrum was used as the light source for the characterizations and the device temperature was kept at 25°C. After the first measurement, the solar cells were kept in a clean-room environment for 5 months and were then measured again in order to study the impact the plasma damage and hydrogen addition over time. Since, the V_{oc} changes measured are usually quite small, [10] at least three solar cells for each combination of pitches and hydrogen fractions were fabricated and measured in order to ensure that the small changes measured were reproducible. The V_{oc} values presented are the average of the V_{oc} of all the cells of a specific pitch and hydrogen fraction combination.

3. Results and discussion

3.1. III-V/Ge etching process characterization

3.1.1. Impact of temperature with a pure $SiCl_4$ plasma

First, the impact of the cathode temperature on the etch morphology for a pure $SiCl_4$ plasma was studied. Fig. 5 presents cross-section SEM images as a function of the cathode temperature of the etched patterns with a pure $SiCl_4$ plasma. It shows a degradation of the heterostructure profile with increased temperature. As shown in Fig. 6, the lateral erosion of Ge and (In)GaAs layers gradually increases with temperature (from 100 nm to 3 μm). The In-rich InGaP erosion is absent below 150°C and it skyrockets to 10μm at 200°C. Isotropic etching results from the chemical action of chlorine radicals, which is known to be activated by temperature, explaining the lateral etch rate increase. [27,29] As for the In-rich InGaP, $InCl_x$ are supposed to be the etch byproducts, which volatility limits InGaP etching at low temperature and those compounds become volatile above 150°C. [1,8] This explains why the InGaP lateral etching is considerably enhanced above 150°C. Fig. 6 also shows an increase of the vertical average etch rate of the heterostructure with temperature, which is mainly attributed to the activation of the vertical etching of the InGaP layer. In combination with the SiO_2 etch rate reduction at high temperature, as shown in Fig. 7, the III-V/Ge over SiO_2 etch selectivity increases with temperature. The SiO_2 etch rate reduction at high temperature can be explained by the enhanced deposition of $SiCl_x$ species, as previously reported in $SiCl_4$-based plasma-enhanced chemical vapor deposition. [20] Furthermore, a high temperature could promote desorption of the reactive species before they can react with the SiO_2 surface, which could also lead to a reduced SiO_2 etch rate. Such mechanism was previously observed in NH_3/NF_3 plasma etching of Si_3N_4 [30].

Despite the isotropic behaviour observed at higher temperature, there is a deposition of etch inhibitors on the pattern sidewalls (or etch-inhibiting layer) that can be observed. At 20°C, an inhibiting layer with an homogeneous thickness (100 nm) along the sidewalls is observed on the STEM image presented in Fig. 8 b). By increasing the temperature, the inhibiting layer becomes spatially localised on the (In)GaAs region and can be several micrometers thick, as shown on the SEM-EDX image in Fig. 9. This layer seems porous and ex-situ EDX reveals a SiO-like chemical composition although no oxygen is voluntary introduced. A similar chemical composition is detected at all temperatures. Despite the fact that no chlorine is detected, it is likely that a $SiCl_x$ layer is deposited while the etch is performed.

Oxygen can be added to the inhibiting layer during the etching process, whether it was coming from the reactor walls, [3] or from the SiO_2 cover plate etching. The released oxygen can oxidize the deposited $SiCl_x$ on the sidewalls, forming a SiO_xCl_y-like layer. It can then turn into a more SiO_x-like layer after air exposure since the reaction with ambient air is not controlled. This reaction can be explained by a substitution of chlorine by oxygen. [4,12] The SiO_2 cover plate etching (Fig. 7) creates an atomic oxygen flux (Φ), which can be estimated by using the following equation:

$$\Phi = \frac{\rho SE}{(f_{Si} m_{Si} + f_O m_O)} V_m F_O \quad (1)$$

In this equation, Φ is the atomic oxygen flux (in sccm), ρ is the SiO_2 density (2.2 $\frac{g}{cm^3}$), S is the cover plate area exposed to the plasma (78.5 cm^2), E is the etch rate of the SiO_2 cover plate (70–120$\frac{nm}{min}$), f_{Si} and f_O are the atomic percentage of silicon and oxygen in the cover plate respectively ($\frac{1}{3}$ and $\frac{2}{3}$), m_{Si} and m_O are the silicon and oxygen molar masses respectively (28.09 $\frac{g}{mol}$ and 16 $\frac{g}{mol}$), V_m is the molar volume for an ideal gas (22,400 $\frac{cm^3}{mol}$) and F_O is the fraction of the etched byproducts contributing towards the atomic oxygen flow ($\frac{2}{3}$). From this estimation, an oxygen equivalent atomic flux of 1.5 sccm is probably added to the plasma at 20°C and it decreases to 0.9 sccm at 200°C since the SiO_2 etch

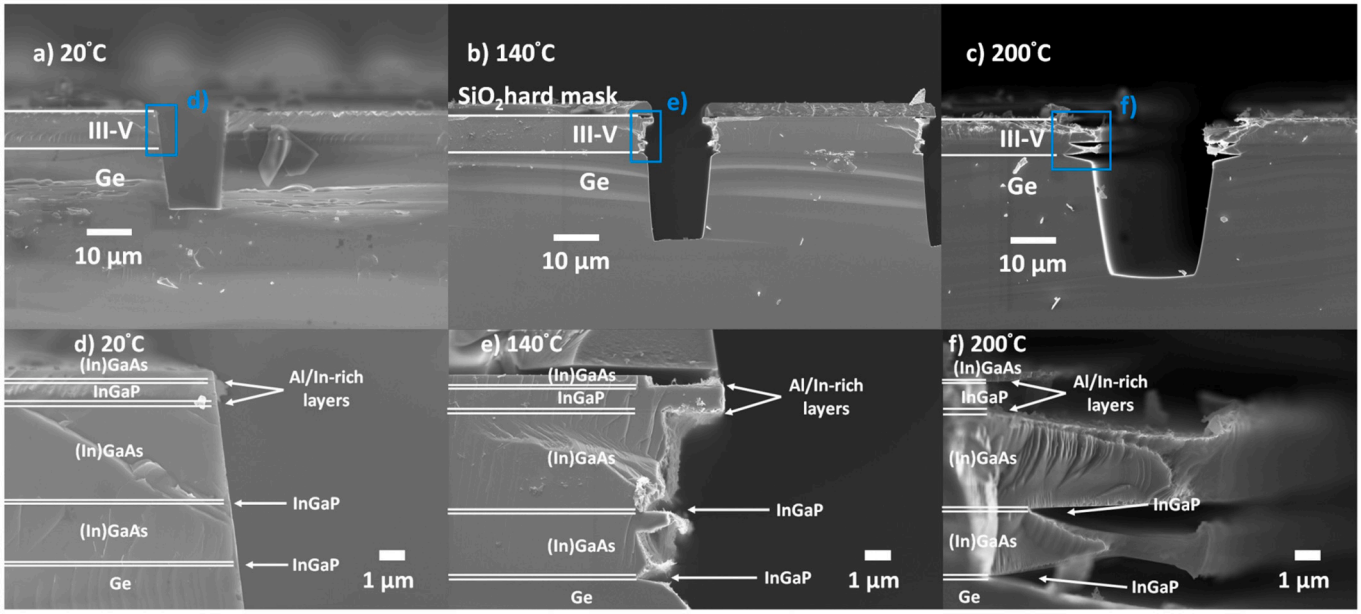

Fig. 5. Cross-section SEM images of the patterns etched with a pure $SiCl_4$ plasma at a) 20˚C, b) 140˚C and c) 200˚C. Fig. 5 d), e) and f) are close-ups of the sidewalls etched at 20˚C, 140˚C and 200˚C respectively. It can be noted that, at 140˚C, the (In)GaAs layers with low indium concentration exhibit a larger sidewall erosion than the In-rich InGaP layers. This trend is reversed at 200˚C, as the In-rich InGaP layers exhibit a larger sidewall erosion than the (In)GaAs layers.

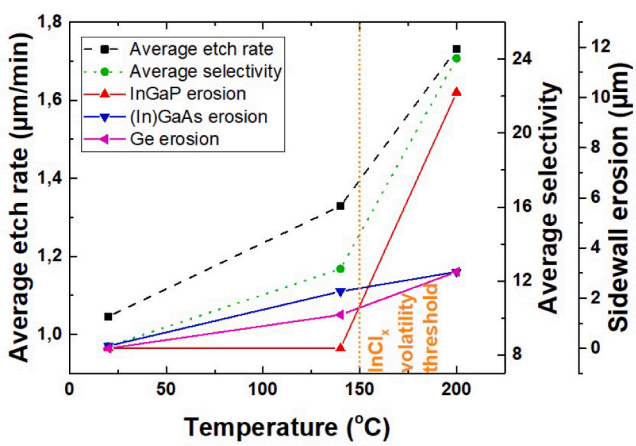

Fig. 6. Average etch rate, selectivity and sidewall erosion of the main semiconductors in the heterostructure obtained with a pure $SiCl_4$ plasma as a function of the cathode temperature.

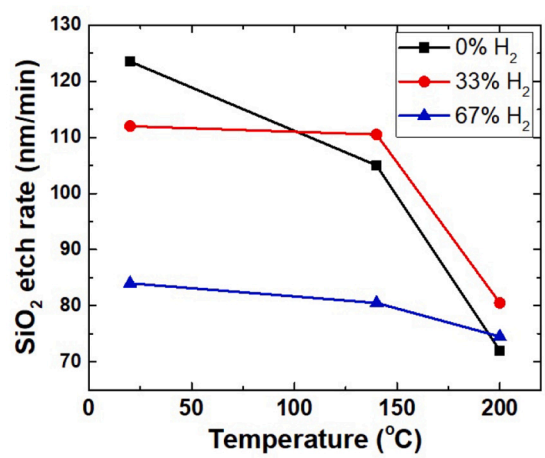

Fig. 7. SiO_2 etch rate in $SiCl_4/H_2$ as a function of the cathode temperature.

rate decreases from 120 to 70$\frac{nm}{min}$, which confirms that oxygen can be incorporated into the inhibiting layer in these conditions. These gas flows represent less than 8% of the total gas flow, which is clearly not negligible nor controlled during the process. The oxygen content could be controlled by adding a small oxygen flow, which could improve the control over the process. However, no oxygen flow was intentionally added as both oxygen and hydrogen can not be used simultaneously.

As for the specific deposition mechanism, the inhibiting layer species can come from the sputtering of the bottom of the etched features in a direct line of sight or come from the plasma gas phase (both the etch byproducts or gas phase condensation). [21,26] Species coming from the sputtering of the etched features tend to deposit a conformal layer on the sidewalls. This deposition mechanism could explain the homogeneous thickness of the inhibiting layer obtained at 20˚C. On the other hand, species coming from the plasma gas phase tend to form thicker layers on the top of the sidewalls than on the bottom. Such mechanism is mainly responsible for the formation of the inhibiting layer at 200˚C since no layer was formed on the Ge, at the bottom of the sidewalls. The species coming from the SiO_2 hard mask etching do not seem to drive the inhibiting layer deposition rate since the SiO_2 etch rate reaches a minimal value at 200˚C (Fig. 7). Consequently, the gas phase species from the $SiCl_4$ precursor drive the inhibiting layer formation at high temperature.

The temperature alters the deposition mechanisms since the thin layer with an homogeneous thickness (100 nm) obtained at 20˚C becomes thicker (4μm) spatially localised on the (In)GaAs layers at 200˚C. This behaviour indicates that there is a competition between the sidewall erosion, driven by the atomic chlorine, and the $SiCl_x$ species deposition. At 20˚C, the inhibiting layer is porous (Fig. 8 b), which explains why there is a small sidewall erosion on the (In)GaAs layer. Since the In-rich InGaP erosion is thermally activated, the lateral etching exceeds the deposition at 200˚C, preventing the formation of an inhibiting layer in this vicinity. Two mechanisms can explain why a thicker (4μm) layer is formed at high temperature on the (In)GaAs sidewalls: (1) the deposition rate is increased at high temperature, as previously reported

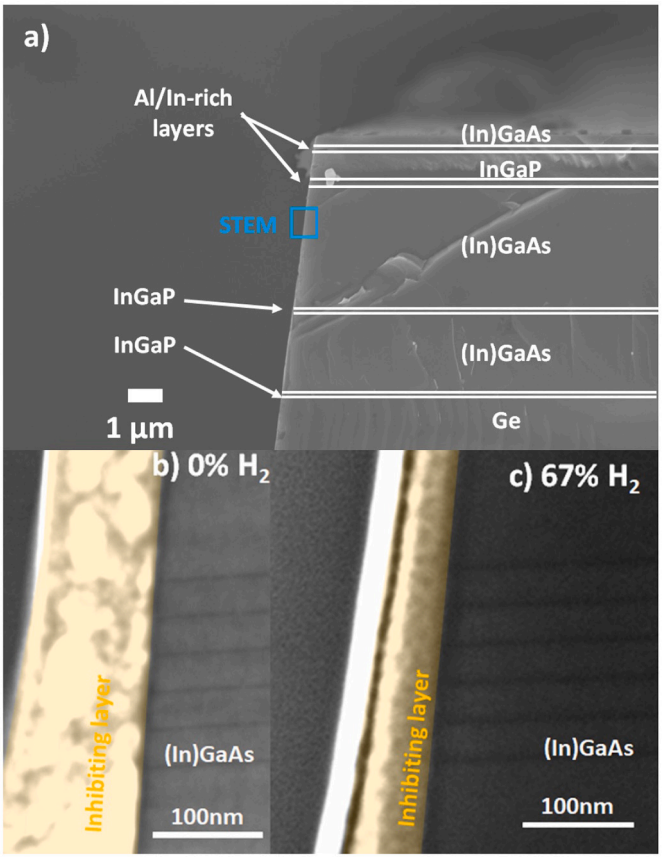

Fig. 8. Cross-section STEM images in the vicinity of the inhibiting layer of the (In)GaAs middle cell. Fig. 8 a) is a SEM image presenting the area sampled by STEM. The patterns were etched at 20°C with $SiCl_4$ and a) 0% b) 67% H_2 fraction of the total gas flow.

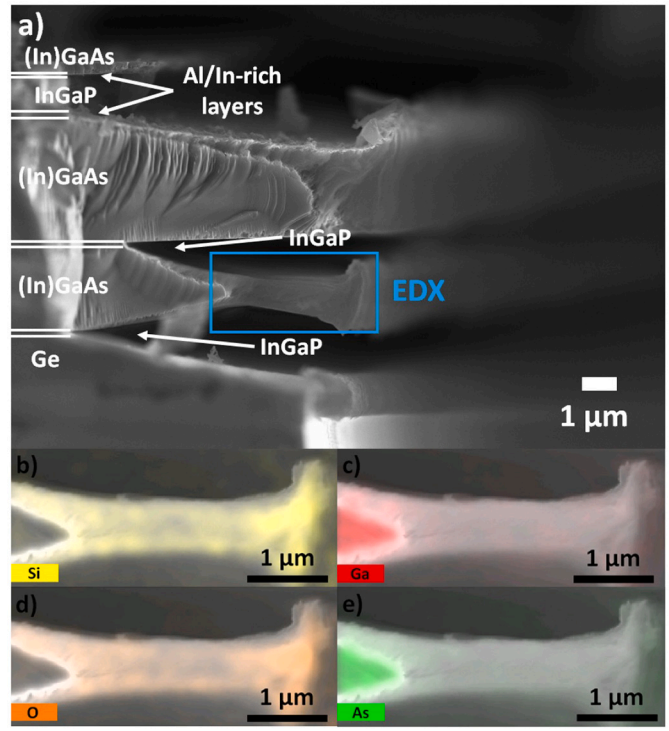

Fig. 9. EDX cartography of the patterned sidewall and its inhibiting layer in the vicinity of an (In)GaAs layer etched with a pure $SiCl_4$ plasma at 200°C. Fig. 9 a) is a SEM image presenting a close-up of Fig. 5 c) and it presents the area sampled by EDX whereas Fig. 9 b), c), d), e) present the EDX intensities associated to Si, Ga, O and As respectively.

in $SiCl_4$-based plasma-enhanced chemical vapor deposition [20] and (2) the isotropic morphology shields the inhibiting layer from the plasma ion bombardment.

3.1.2. Impact of hydrogen addition at 200°C

The hydrogen addition to the gas flow was also investigated. Fig. 10 presents cross-section SEM images of the etched patterns and Fig. 11 presents the average etch rate, the average selectivity and the sidewall erosion of the InGaP, the (In)GaAs and Ge layers for a $SiCl_4/H_2$ plasma at 200°C with different hydrogen fraction to the total gas flow (0%, 33% and 67%). When hydrogen is added to the plasma mixture, the sidewall erosion is reduced below $<1\mu m$ for all the III-V materials and it is completely eliminated in the vicinity of the Ge substrate. As shown in Fig. 11, the average etch is also signficantly reduced by increasing the H_2 flow (from $1.7\frac{\mu m}{min}$ to $450\frac{nm}{min}$). However, H_2 addition at 200°C does not alter the SiO_2 hard mask etch rate ($(76\pm4)\frac{nm}{min}$, Fig. 7). Therefore, the III-V/Ge over SiO_2 selectivity drops from 24 to 6 by adding hydrogen to the plasma mixture (Fig. 11).

Hydrogen addition has two major impacts on the plasma process: (1) it decreases the chlorine radical flux by scavenging atomic chlorine and (2) it enhances the $SiCl_x$ species deposition [5,11,16,20] As a matter of fact, it was reported that a high hydrogen fraction can completely swap the process regime from etching to deposition. [5] Both of these mechanisms can be understood with the following equations:

$$SiCl_x \rightarrow SiCl_{x-1} + Cl \quad (2)$$

$$H + Cl \rightarrow HCl \quad (3)$$

At high hydrogen fraction, the hydrogen eliminates the atomic chlorine within the plasma. [5] A smaller chlorine radical flux reduces the chemical etching of the process, which explains the reduction in both the sidewall erosion and the average etch rate (Fig. 11). Such mechanism was previously observed on InP/InGaAs and InP/InGaAlAs heterostructure plasma etching. [19] The ratio of the sidewall erosion over the etched depth is reduced with increasing hydrogen flow, which leads to an etching process that is, overall, more anisotropic.

The inhibiting layer thickness and morphology are significantly altered by increasing the hydrogen fraction. The inhibiting layer thickness is first reduced (33% H_2), to finally disappear from the (In)GaAs sidewalls at 67%. In the latter conditions, it is now spatially localised on the InGaP sidewalls and its thickness does not exceed 200 nm (not shown here). This thickness reduction can be explained by the fact that the precursor flow has been reduced threefold. This is consistent with a previous article that showed that the deposition rate in $SiCl_4/H_2$ PECVD is first increased with hydrogen flow but then falls off after surpassing a critical hydrogen flow. [20] This is further confirmed by another study that has shown that the deposition rate is linearly related to the product of H and $SiCl_x$ in the gas phase and that there is an optimal $H_2/SiCl_4$ ratio, for which, the deposition rate is maximized. [5] The hydrogen addition changes severely the deposition mechanism since the hydrogen atoms can induce the free-bond silicon species, which are involved in the growth process. [5] In this present study, the optimal deposition rate may have been surpassed, which can explain the inhibiting layer thickness reduction. Furthermore, the SiO_2 hard mask etching can not explain the changes in the inhibiting layer thickness. Indeed, the SiO_2 hard mask etch rate, and its associated oxygen atomic flow remains about the same with H_2 addition at 200°C ($(76\pm4)\frac{nm}{min}$, Fig. 7).

3.1.3. Impact of hydrogen addition at 20°C

Hydrogen has also been added to the gas flow of the processes performed at 20°C. Fig. 12 presents cross-section SEM images of the etched patterns and the sidewalls are all steep, which confirms that a

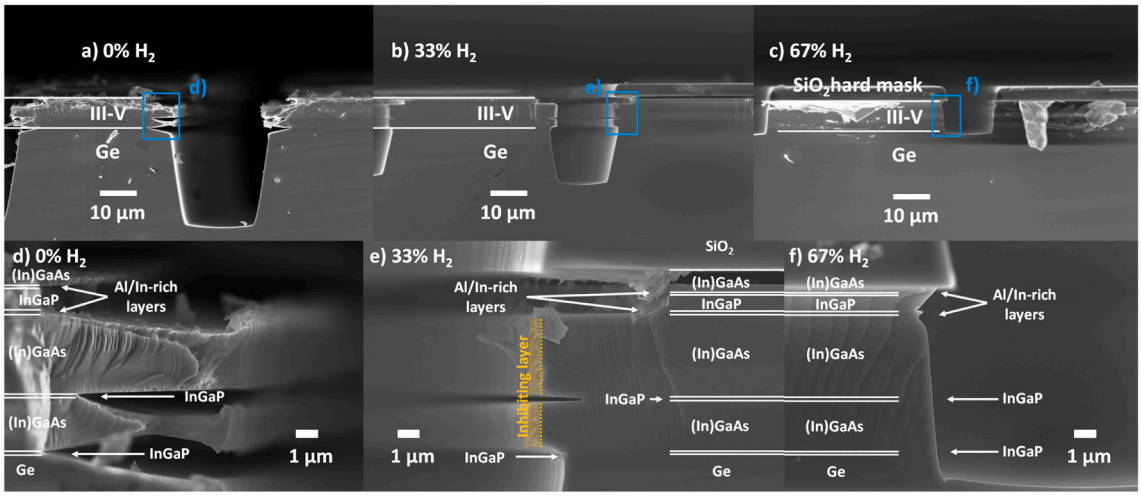

Fig. 10. Cross-section SEM images of the patterns etched at 200°C with $SiCl_4$ and a) 0%, b) 33% and c) 67% H_2 fraction of the total gas flow. Fig. 10 d), e) and f) are close-ups of the sidewalls etched at 200°C with $SiCl_4$ and a) 0%, b) 33% and c) 67% H_2 fraction of the total gas flow.

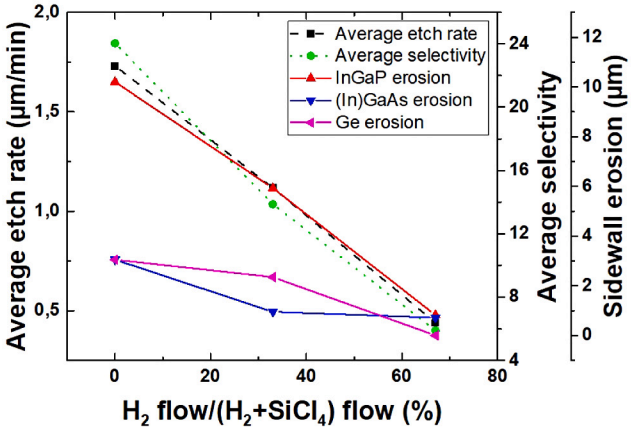

Fig. 11. Average etch rate, selectivity and sidewall erosion of the main semiconductors in the heterostructure, obtained at 200°C with a $SiCl_4/H_2$ plasma as a function of the percentage of the hydrogen flow to the total flow.

temperature of 20°C limits the chemical etching. Fig. 13 presents the average etch rate, the average selectivity and the sidewall erosion of the (In)GaAs and the Al-rich layers layers for a $SiCl_4/H_2$ plasma at 20°C with different hydrogen fractions to the total gas flow. By adding hydrogen, the average vertical etch rate is decreased by 57% to reach ~450$\frac{nm}{min}$ and it can be explained by the same mechanism presented above: the hydrogen scavenges the atomic chlorine and it limits the chemical etching. Furthermore, since all experiments are performed at a fixed pressure, adding hydrogen implies that the $SiCl_4$ flow must be reduced. This will reduce the partial pressure associated to Cl-based species and therefore, the heterostructure etch rate as well. This characteristic provides a second explanation on the origin of the reduced etch rate. This etch rate reduction is less significant at 20°C than 200°C (75%) since chemical etching is less dominant without thermal activation. Interestingly, the etch rates at 200°C and 20°C are identical when hydrogen consists in 67% of the total gas flow. It demonstrates that the thermal activation no longer drives the average etch rate at a high hydrogen gas flow. Hydrogen addition at 20°C reduces the SiO_2 hard mask etch rate (from 125$\frac{nm}{min}$ at 0% H_2 to 85$\frac{nm}{min}$ at H_2, Fig. 7). However, the III-V/Ge over SiO_2 selectivity is mainly driven by the heterostructure etch rate reduction since it drops from 8.5 to 5.3 by adding hydrogen to the

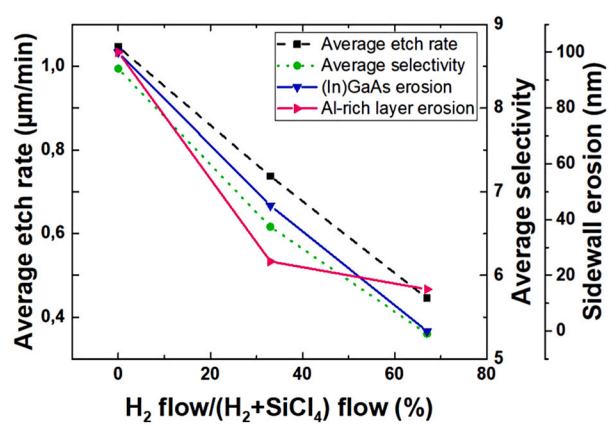

Fig. 13. Average etch rate, selectivity and sidewall erosion of the main materials obtained at 20°C with a $SiCl_4/H_2$ plasma as a function of the percentage of the hydrogen flow to the total flow.

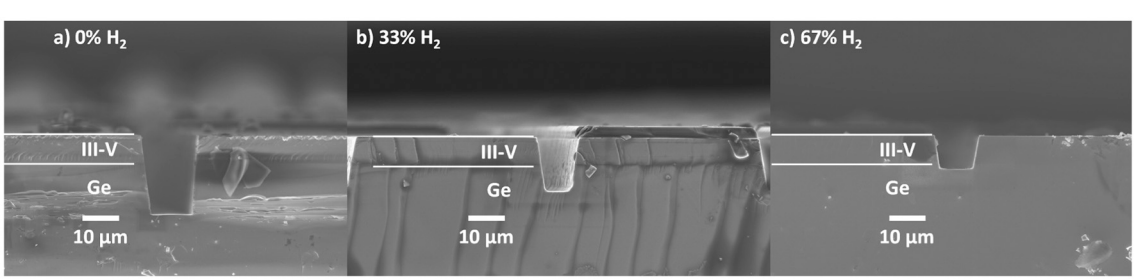

Fig. 12. Cross-section SEM images of the patterns etched at 20°C with $SiCl_4$ and a) 0%, b) 33% and c) 67% H_2 fraction of the total gas flow.

plasma mixture. As presented in Fig. 14, only the (In)GaAs and several Al-rich layers were slightly eroded, whereas both the InGaP and the Ge do not present sidewall erosion at 20˚C. The erosion is reduced to 0 and 15 nm for the (In)GaAs and the Al-rich layers respectively by increasing the hydrogen flow up to 67% (Fig. 13) and it is yet another outcome of chlorine scavenging with hydrogen.

Fig. 15 presents a TEM-EDX cartography of the (In)GaAs sidewall and its inhibiting layer after an etching process performed at 20˚C and with 67% H_2. As the hydrogen fraction is increased, the inhibiting layer is still conformal and protects all the layers but it becomes less porous, as shown in Fig. 8 c). This characteristic occurs because the reduced chemical etching creates less competition with the deposition. The hydrogen addition also creates a denser layer by scavenging some of the chlorine directly from the inhibiting layer [11,16] with the following reaction:

$$SiCl_x + H \rightarrow SiCl_{x-1} + HCl \quad (4)$$

This inhibiting layer has a 50 nm thickness, which is thinner than its 200˚C counterpart (~200nm). However, it is impossible to comment on

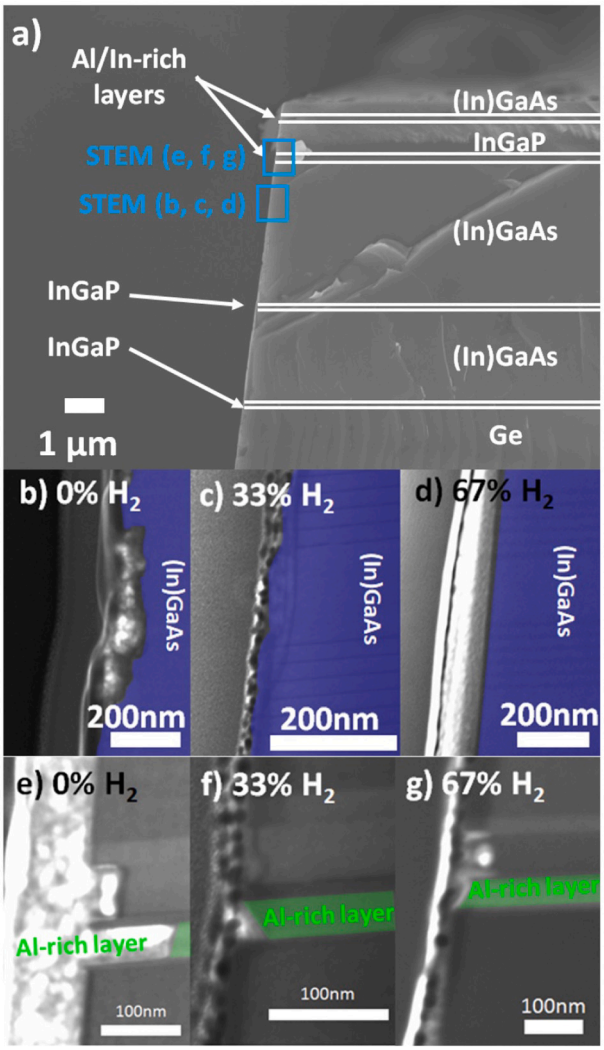

Fig. 14. Cross-section STEM images performed on the etched sidewall. Fig. 14 a) is a SEM image presenting the areas analyzed by STEM. The STEM images were performed in the vicinity of the (In)GaAs middle cell of the patterns etched at 20˚C with $SiCl_4$ and b) 0% c) 33% and d) 67% H_2 fraction of the total gas flow as well as in the vicinity of the Al/In-rich layers of the patterns etched at 20˚C with $SiCl_4$ and e) 0%, f) 33% and g) 67% H_2 fraction of the total gas flow.

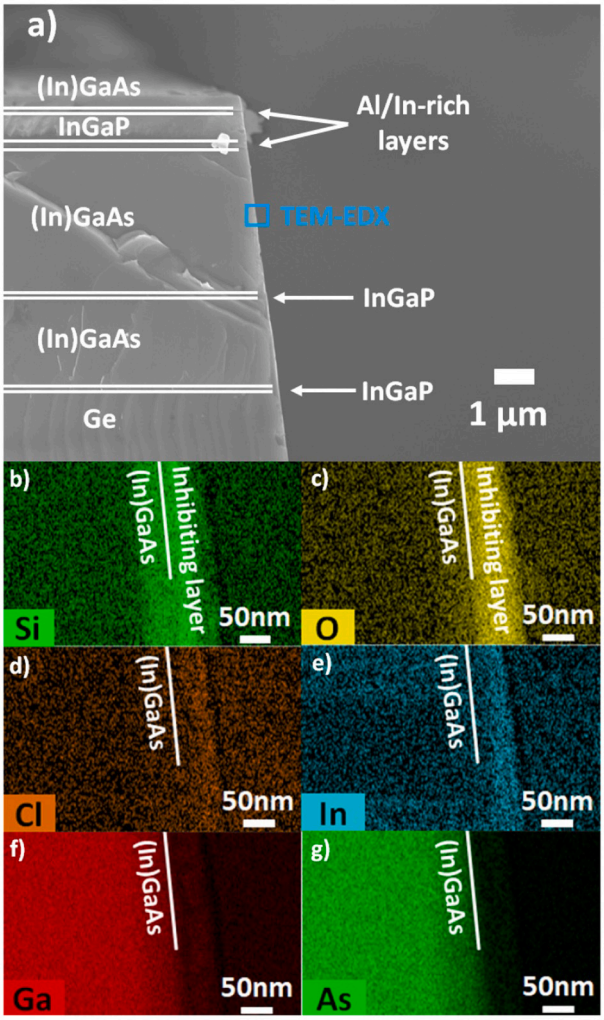

Fig. 15. TEM-EDX cartography of the sidewall and its inhibiting layer in the vicinity of an (In)GaAs layer etched with a $SiCl_4$ and H_2 (67% of the total gas flow) plasma at 20˚C. The SEM image on Fig. 15 a) presents the area analyzed by TEM-EDX whereas Fig. 15 b), c), d), e) f) and g) present the EDX intensities associated to Si, O, Cl, In, Ga and As respectively.

the $SiCl_x$ deposition rate based solely on these thicknesses since the porosity is highly affected and it creates a significant margin of error (>50%) in this assessment. As for its atomic composition, this layer consists of mostly silicon and oxygen by the same mechanism explained beforehand. However, both indium and chlorine can also be observed in this layer, which was not observed under any other conditions. Their addition indicates the formation of $InCl_x$ clusters coming from the In-based semiconductor etching with the chlorine-based plasma. The sputtering of the bottom of the etched features, combined with the low $InCl_x$ volatility at 20˚C, explains their addition to the inhibiting layer.

3.1.4. III-V/Ge sidewall composition

The atomic composition of the sidewall was further investigated by time-of-flight secondary ion mass spectrometry (ToF-SIMS). Before the measurement, the inhibiting layer was stripped with diluted HF. This way, it is possible to study the elements that may have been incorporated into the III-V/Ge sidewall during the plasma process. Fig. 16 presents the average chlorine ion intensity taken from the sidewalls as a function of the depth into the etched III-V/Ge sidewall for all three processes performed at 20˚C. The samples etched at both 140˚C and 200˚C were not studied as the sidewall erosion is not suitable for the final application. For a pure $SiCl_4$ plasma, a high amount of chlorine is

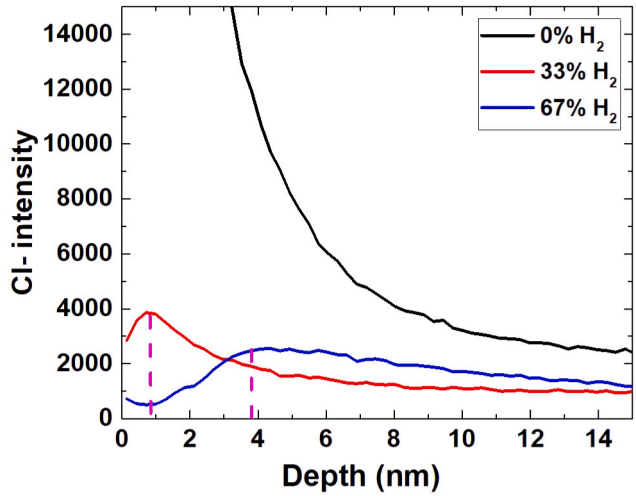

Fig. 16. ToF-SIMS measurement of the average chlorine ion intensity taken from the sidewalls measured as a function of the depth into the etched III-V/Ge sidewall for different hydrogen fraction of the total gas flow. The measurement was performed after the inhibiting layer removal.

incorporated into the III-V/Ge sidewall. As expected, the chlorine concentration decreases with the depth into the etched sidewall. Chlorine concentration decreases with hydrogen addition and it is mainly located within the first 1 nm. At 67%, it seems that chlorine penetration depth is more spread. The reduced chlorine concentration can be explained by the chlorine atom scavenging by the hydrogen. Furthermore, since adding hydrogen requires reducing the $SiCl_4$ flow in order to keep both a fixed pressure and a fixed total gas flow, there will be less Cl-based species available in the plasma. Both of these characteristics reduce the amount of atomic chlorine atoms in the plasma that are available to be incorporated into the sidewall. It was previously shown that chlorine diffusion in III-V materials may create Cl-related defects. [25] Therefore, this mechanism could also reduce the Cl-related defect density.

Fig. 17 presents the average hydrogen ion intensity taken from the sidewalls as a function of the depth into the etched III-V/Ge sidewall for all three processes performed at 20°C. For a pure $SiCl_4$ plasma, a low amount of hydrogen is incorporated in the III-V/Ge sidewall. Since no hydrogen was intentionally added for this process, this low amount can

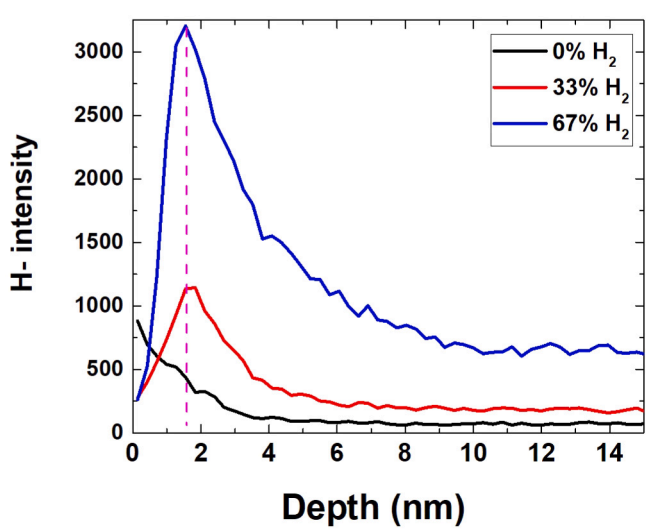

Fig. 17. ToF-SIMS measurement of the average hydrogen ion intensity taken from the sidewalls measured as a function of the depth into the etched III-V/Ge sidewall for different hydrogen fraction of the total gas flow. The measurement was performed after the inhibiting layer removal.

be attributed to residual hydrogen within the ToF-SIMS chamber. A larger amount is incorporated with the plasma etching process with 33% H_2. The hydrogen concentration within the III-V/Ge sidewall is even larger when the hydrogen fraction is raised from 33% to 67%. In both the later cases, the maximum concentration is located 2 nm beneath the sidewall surface.

3.1.5. *Sidewall plasma damage*

To further study these properties, cathodoluminescence measurements were performed on the III-V semiconductor plasma-etched sidewalls after the inhibiting layer removal. Fig. 18 presents the cathodoluminescence intensity of the InGaP top cell as a function of the photon energy for the pure $SiCl_4$ process (0%), the process with 67% H_2 performed at 20°C and a cleaved sidewall used as a reference. The maximum peak intensity is reached at ~1.84 eV which is consistent with the InGaP band gap energy. It is possible to notice that the intensity is at least twice as large with any plasma process instead of the cleaved sample. This is a first indication that the plasma process does not damage much the heterostrucure in the vicinity of the InGaP top cell. However, the cathodoluminescence intensity is increased by 700% when a high hydrogen fraction is added when compared to the cleaved sidewall. Such behaviour can be explained by a reduction of the non-radiative defect on the InGaP sidewall. This characteristic is in agreement with the ToF-SIMS results. The high hydrogen fraction within the plasma helps scavenging the chlorine which reduces the Cl-induced non-radiative defects. Furthermore, the hydrogen incorporation into the sidewalls (Fig. 17) can passivate impurities or vacancy-related recombination centers. Hydrogen can passivate impurities in semiconductors as previously shown on Si [6] and GaAs. [22] In addition, it has been observed that, after GaN plasma etching, a hydrogen plasma passivates the nitrogen vancancies, which also leads to a luminescence increase. [7] The authors also observed that a high hydrogen-radical-to-ion flux ratio is preferable to maximize the passivating properties on GaN. In the case of our study, since the sidewalls are investigated, the geometry naturally promotes a high neutral-to-ion flux ratio in this vicinity. Despite the fact that InGaP and (In)GaAs were studied in this work, it is possible that a similar passivation process occurred. This property provides a second explanation on the 700% luminescence increase shown in Fig. 18. Both the previous publications and the results of this study suggest a specific passivation mechanism. The hydrogen radicals passivate the impurities or vacancy-related recombination centers, whereas the geometry enables an ion flux at grazing angle on the sidewalls, which limits the dissociation of the newly-formed bonds with hydrogen.

Fig. 19 presents the cathodoluminescence intensity of the (In)GaAs

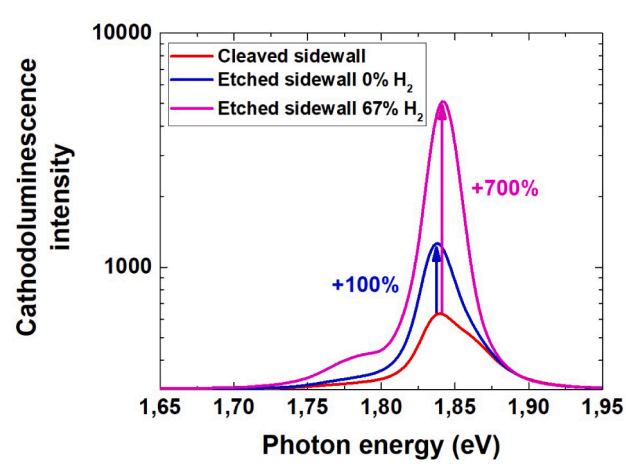

Fig. 18. Cathodoluminescence intensity of the InGaP top cell as a function of the photon energy. The measurement was performed after the inhibiting layer removal.

middle cell as a function of the photon energy for the pure $SiCl_4$ process (0%), the process with 67% H_2 performed at 20°C and a cleaved sidewall used as a reference. The maximum peak intensity is reached at ~1.4 eV which is consistent with the (In)GaAs band gap energy. The peak intensity variation associated to the (In)GaAs middle cell does not vary more than 30% between all three samples. Therefore, the luminescence peak does not change much whether the sample was cleaved, plasma etched or even when hydrogen was added. In the vicinity of the (In)GaAs layers, no benefits from the hydrogen addition could be observed. This result is not consistent with a previous publication indicating that hydrogen plasmas have passivating properties by removing an arsenic excess and its associated native oxide (As_2O_3). [18] A similar mechanism was also reported for GaAs passivation with silicon nitride by PECVD. [32] In the case of this study, the etched sidewall does not have a native oxide since it was still considered bulk before the process. Therefore, the hydrogen had no native oxide to react with. Hydrogen could still remove an arsenic excess on the etched sidewall. [18] However, the cathodoluminescence results indicate that this passivation mechanism was poorly efficient (Fig. 19). An explanation for this could be that the As-excess was not completely removed during the plasma etching process. This explanation is consistent with the etching sequence of the heterostructure (Fig. 2). The InGaP top cell is the first subcell to be etched and it has the slowest etch rate. During this part of the process, the (In)GaAs sidewalls can not be passivated since this layer is not etched yet. The (In)GaAs middle cell is the second subcell to be etched, during which, the top cell sidewalls are still exposed to the plasma and its passivating properties. This means that the InGaP sidewalls are exposed to the plasma for a greater period of time than the (In)GaAs middle cell. Consequently, the InGaP top cell received a complete passivation resulting in a 700% luminescence increase (Fig. 18), whereas the middle cell had an incomplete passivation because a large fraction of the process was required to etch the top cell and it leads to no significant changes in cathodoluminescence (Fig. 19).

Secondary peaks between 1.45 eV and 1.5 eV can also be observed in Fig. 19. They may come from the interactions of different III-V materials both above and below the (In)GaAs layers. Because of the intricacy of the heterostructure studied, no specific identification or explanation for those secondary peaks can be provided in the scope of this study. A separate study on isotype substrates will be required to rigorously identify these secondary peaks and the associated etching mechanisms.

3.2. Solar cell performance characterization

Fig. 20 presents the one-sun AM1.5D open-circuit voltage of multijunction solar cells with vias with different via pitches (60μm, 80μm and 100μm) compared to multijunction solar cells without via-holes (Ref). Both the vias and the isolating trenches were etched with either a pure $SiCl_4$ plasma (0%) or with a high hydrogen fraction (67%). A first measurement was performed right after the fabrication cycle (T_0) and the via-hole etching process induces a relative V_{oc} loss between 2% and 3%. These values are in agreement with previous studies. [10] However, a slightly smaller loss (~2%) is obtained when a high hydrogen flow (67%) is used instead of a pure $SiCl_4$ plasma (~3%). These measurements are below the precision of the measurement setup. In order to confirm that the hydrogen addition has also a positive effect on the open-circuit voltage, a good level of reproductibility was obtained. At least three solar cells for each pitch and hydrogen fraction combination, for a total of 24 solar cells, were fabricated and measured. All the solar cells of each subset present the same V_{oc} within 0.1% and 0.8%. These values are all below the V_{oc} changes associated to hydrogen addition and for all the via pitches studied. Therefore, the smaller V_{oc} loss associated to hydrogen addition is real and not simply a statistical artifact.

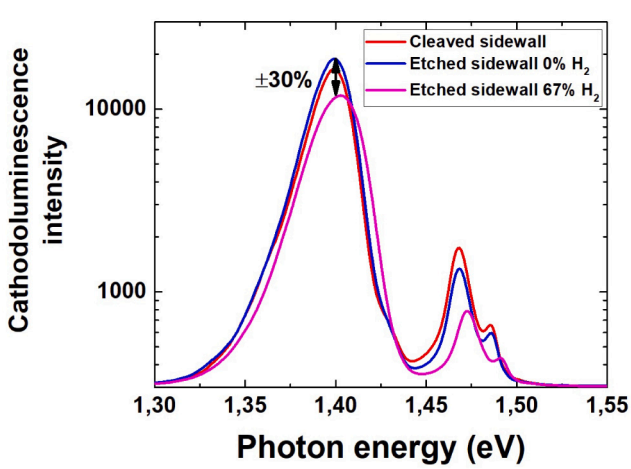

Fig. 19. Cathodoluminescence intensity of the (In)GaAs middle cell as a function of the photon energy. The measurement was performed after the inhibiting layer removal.

Furthermore, it is possible to notice that, for both the cells with vias and the reference cells, when a high hydrogen flow is used, a higher open-circuit voltage is obtained. The passivating properties of this process is also observable on the standard reference cells since the mesa etching step used to electrically isolate one cell to another is also performed by the same plasma etching process. This result is of interest even beyond the fabrication of the through cell via contact architecture. It provides an appealing pathway to increase the conversion efficiency of III-V based solar cells with standard contacts since this step is usually performed by wet chemical etching on state-of-the-art multijunction solar cells [13,17].

The enhanced open-circuit voltage with hydrogen can be explained by the quality of the etched sidewalls. A reduction of the non-radiative defect density reduces the recombination at the edge of the device and it results in a higher open-circuit voltage. This result provides a solid confirmation for the mechanism presented by the ToF-SIMS and cathodoluminescence measurements in the previous sections. Indeed, it was previously observed that hydrogen passivate defect-related recombination centers on solar cells resulting in a higher conversion efficiency. [35,36] A slight V_{oc} increase can be observed as the pitch is increased from 60μm to 100μm on the cells with vias etched with a pure $SiCl_4$ plasma. This is related to the reduction of the perimeter-to-area-ratio with increasing via pitch. As the perimeter-to-area of the device decreases, the total sidewall recombination is less dominant and the solar cell presents a higher V_{oc}. However, this behaviour is not noticeable on the cells with via-holes etched with a high hydrogen fraction. The V_{oc} does not seem to change much by increasing the via pitch and this may also be explained by an efficient sidewall passivation. With the defect passivation, the complete device is less sensitive to perimeter-to-area effect, hence the steady V_{oc} over all the studied via pitches.

One of the challenges with passivation is to ensure that it has a good stability over time. Therefore, these characterizations were also performed five months after the initial measurement in order to assess the stability of the hydrogen passivation. The results are also presented in Fig. 20 (T_0+5 months). For all the samples studied, the influence of the hydrogen addition to the plasma mixture is still noticeable after five months. Indeed, all the solar cells etched with a high hydrogen fraction plasma still exhibit a higher open-circuit voltage when compared to their solar cell counterpart etched with the pure $SiCl_4$ process. The impact of via-hole etching remains the same after five months as the relative V_{oc} loss is still between 2% and 3%. Furthermore, the relative loss associated to via-hole etching is still lower when hydrogen is added to the plasma mixture (2.1–2.7% depending on the via pitch) compared to the pure $SiCl_4$ plasma (2.3–2.9% depending on the via pitch). Since solely the hydrogen addition to the plasma mixture can explain this behaviour, this result indicates that the hydrogen plasma passivation persists over time for at least 5 months. The long-lasting stability of

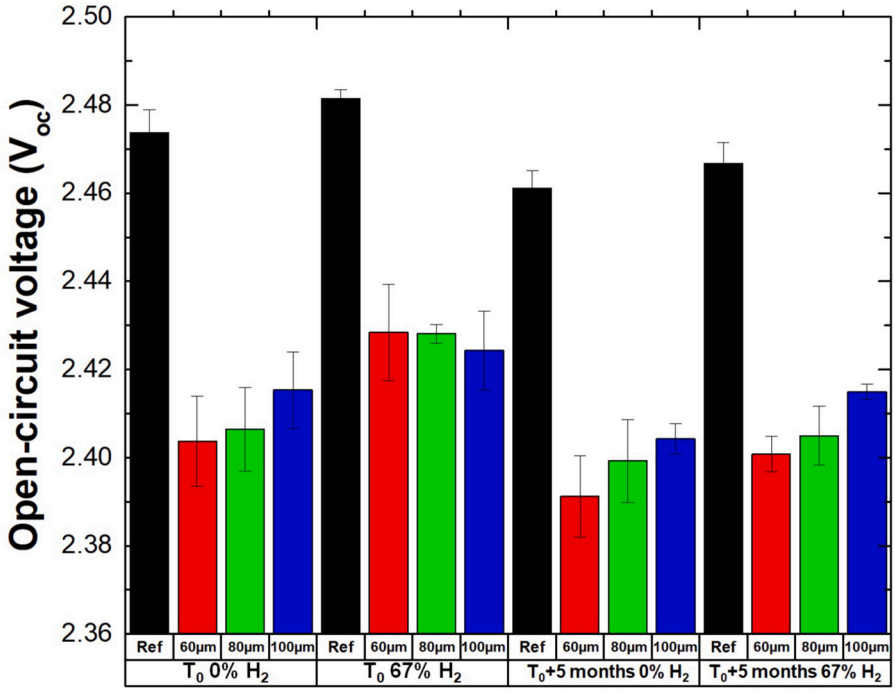

Fig. 20. Open-circuit voltage of multijunction solar cells with vias with different via pitches (60μm, 80μm and 100μm) compared to multijunction solar cells without via-holes (Ref). Both the vias and the isolating trenches were etched with either a pure $SiCl_4$ plasma (0%) or with a high hydrogen fraction (67%). The measurements were performed right after the fabrication cycle (T_0) and after 5 months (T_0 + 5 months).

hydrogen-based passivation was also previously observed in another study. [18] For through cell via contact multijunction solar cells, the via sidewalls will be covered by a dielectric barrier that is expected to further increase the stability of the semiconductor sidewalls.

3.3. Etching process completion

The $SiCl_4/H_2$ process detailed above is only one step (Fig. 3 b) of the full etching process (Fig. 3). The $SiCl_4/H_2$ plasma is solely used to etch the active layers of the III-V/Ge heterostructure without sidewall erosion and with limited plasma damage. To reach those goals, this step was performed with the 67% H_2 process performed at a cathode temperature of 20°C. However, additional steps are required to obtain deep and anisotropic vias through the III-V/Ge heterostructures as shown in Fig. 3. To protect the sidewalls from further damage, a silicon oxide liner is deposited by PECVD (step c in Fig. 3). Then, a CF_4-based plasma process is used to etch the liner at the bottom of the patterns (step d in Fig. 3) by using the same SiO_2 hard mask. Fig. 21 a) presents cross-section SEM images after both the liner deposition and the anisotropic liner etching. Fig. 21 b), c) and d) present close ups of Fig. 21 a) on the sidewall. It is possible to observe that a continuous liner covers all the III-V/Ge sidewall. This demonstrates that the PECVD process is sufficiently conformal to enable deposition on the active layer sidewall, which provides protection against further damage. Moreover, the CF_4 plasma process is sufficiently anisotropic to etch the liner at the bottom of the patterns while keeping the sidewall undamaged.

The last step is a time-multiplexed plasma process to etch the Ge substrate. It consists of a SF_6/O_2 isotropic etching step multiplexed with a C_4F_8 passivation step in order to obtain anisotropic etching. Fig. 22 presents cross-section SEM images of the etched patterns after the Ge etching process (step e in Fig. 3) In Fig. 22 a), it is possible to notice that a depth of 50μm can be obtained with an aspect ratio of 5, but aspect ratios larger than 10 are expected to be reachable with a longer process time. Furthermore, Fig. 22 b) presents a close up view of Fig. 22 a) in the vicinity of the III-V sidewall. After this last step, the liner still protects the sidewall of the active region from plasma damage. In summary,

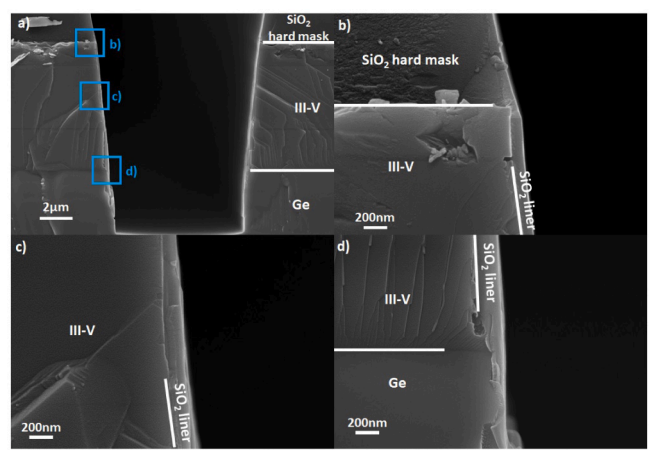

Fig. 21. Cross-section SEM images of the etched patterns after liner deposition and liner etching (step d of Fig. 3).

these last steps enable deep and high aspect ratio etching through the III-V/Ge heterostructure while protecting the active region from further damage.

4. Conclusion

We propose a complete plasma etching process to etch high aspect ratio patterns in III-V/Ge triple junction solar cell heterostructure with low damage for the fabrication of multijunction solar cells. By investigating the influence of H_2 flow and cathode temperature, we demonstrated that the lateral erosion is strongly reduced at low temperature and high H_2 flow. Chlorine radicals scavenging, lower volatility of $InCl_x$ etch by-products and denser inhibiting layer deposition at the pattern sidewall enable a minimal sidewall erosion and steep profiles. The high hydrogen flow reduces the non-radiative defects on the III-V

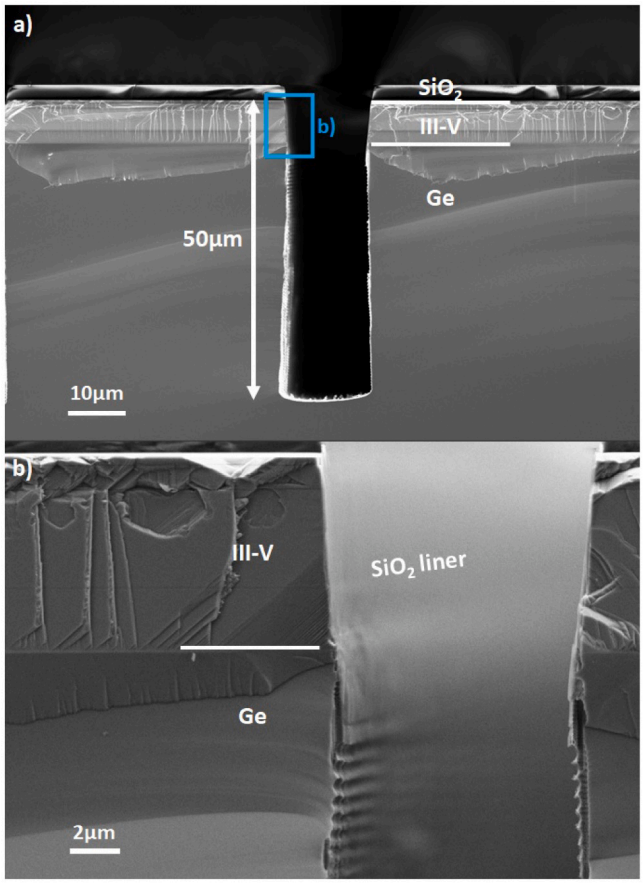

Fig. 22. Cross-section SEM images of the etched patterns after the time-multiplexed Ge etching (step e of Fig. 3).

heterostructure sidewall during the etching process whether it is by integrating III-V materials beyond the inhibiting layer to passivate the residual defects or by scavenging the chlorine atoms, thus preventing the creation of a chlorine-based defect. Consequently, it leads to a higher luminescence in the InGaP top cell. However, no changes were observed in the (In)GaAs middle cell. Nevertheless, the plasma properties were also investigated on triple junction solar cells with via holes. The addition of hydrogen enabled an open-circuit voltage increase (~1%) on all the devices compared to their pure $SiCl_4$ counterpart. The hydrogen passivation seems to also persist over time since the voltage increase was still noticeable after 5 months, which makes it a promising process for complete device fabrication. A SiO_2 liner and a time-multiplexed Ge etching process are also presented in order to etched high aspect ratio patterns while protecting the active region sidewalls. In summary, the best plasma conditions enabled to etch patterns anisotropically through a complex III-V/Ge heterostructure with minimal damage conditions that persist over time. Therefore, this plasma etching process is promising for the fabrication of a through cell via contact architecture on multijunction solar cell but also for conventional triple junction solar cells isolated by plasma etching or for other III-V based photonic applications.

Declaration of Competing Interest

The authors declare that they have no known competing financial interests or personal relationships that could have appeared to influence the work reported in this paper.

Acknowledgement

LN2 is a joint International Research Laboratory (IRL 3463) funded and co-operated by Université de Sherbrooke (Canada) and CNRS (France) as well as INSA Lyon, ECL, UCBL, Université Grenoble Alpes (UGA) as well as the French national nanofabrication network RENATECH. The TOF-SIMS and cathodoluminescence measurements were supported by the French"Recherches Technologiques de Base" program and were performed on the Nano Characterization Platform (PFNC) of the CEA Grenoble. The support from NSERC, Prompt and STACE through the MARS-CPV project is acknowledged. M. de Lafontaine acknowledges FRQNT and Université Grenoble Alpes for financial support. The authors would like to thank T. Chevolleau, T. Charvolin, S. Litaudon and D. Drouin for fruitful discussions.

References

[1] K. Asakawa, T. Yoshikawa, S. Kohmoto, Y. Nambu, Y. Sugimoto, Chlorine-based dry etching of III/v compound semiconductors for optoelectronic application, Jpn. J. Appl. Phys. 37 (1998) 373–387. URL: https://doi.org/10.1143%2Fjjap.37.373, https://doi.org/10.1143/jjap.37.373.

[2] A. Belghachi, S. Khelifi, Modelling of the perimeter recombination effect in gaas-based micro-solar cell, Sol. Energy Mater. Sol. Cells 90 (2006) 1–14. URL: http://www.sciencedirect.com/science/article/pii/S0927024805000309, https://doi.org/10.1016/j.solmat.2005.01.009.

[3] S. Bouchoule, S. Lamkadmi Azouigui, S. Guilet, G. Patriarche, L. Largeau, A. Martinez, L. Legratiet, A. Lemaître, F. Lelarge, Anisotropic and smooth inductively coupled plasma etching of iii-v laser waveguides using hbr-o chemistry, J. Electrochem. Soc. (2008) 155, https://doi.org/10.1149/1.2965790.

[4] S. Bouchoule, G. Patriarche, S. Guilet, L. Gatilova, L. Largeau, P. Chabert, Sidewall passivation assisted by a silicon coverplate during cl2–h2 and hbr inductively coupled plasma etching of inp for photonic devices, J. Vacu. Sci. Technol B: Microelectr. Nanometer Struct. Proces. Measure. Phenomena 26 (2008) 666–674. URL: https://avs.scitation.org/doi/abs/10.1116/1.2898455, https://doi.org/10.1116/1.2898455. arXiv:https://avs.scitation.org/doi/pdf/10.1116/1.2898455.

[5] G. Bruno, P. Capezzuto, G. Cicala, F. Cramarossa, Mechanism of silicon film deposition in the rf plasma reduction of silicon tetrachloride, Plasma Chem. Plasma Process. 6 (1986) 109–125, https://doi.org/10.1007/BF00571271.

[6] K.J. Chang, D.J. Chadi, Theory of hydrogen passivation of shallow-level dopants in crystalline silicon, Phys. Rev. Lett. 60 (1988) 1422–1425. URL: https://link.aps.org/doi/10.1103/PhysRevLett.60.1422, https://doi.org/10.1103/PhysRevLett.60.1422.

[7] S. Chen, K. Ishikawa, Y. Lu, R. Kometani, H. Kondo, Y. Tokuda, T. Egawa, H. Amano, M. Sekine, M. Hori, Individual roles of atoms and ions during hydrogen plasma passivation of surface defects on GaN created by plasma etching, Jpn. J. Appl. Phys. 51 (2012) 111002. URL: https://doi.org/10.1143%2Fjjap.51.111002, https://doi.org/10.1143/jjap.51.111002.

[8] Y.W. Chen, B.S. Ooi, G.I. Ng, C.L. Tan, Electron cyclotron resonance plasma etching of inp through-wafer connections at >4 µm/min using cl2/ar, J. Vacu. Sci. Technol B: Microelectr. Nanometer Struct. Proces. Measure. Phenomena 18 (2000) 1903–1905. URL: https://avs.scitation.org/doi/abs/10.1116/1.1306278, https://doi.org/10.1116/1.1306278. arXiv:https://avs.scitation.org/doi/pdf/10.1116/1.1306278.

[9] M. Darnon, M. de Lafontaine, M. Volatier, S. Fafard, R. Arès, A. Jaouad, V. Aimez, Deep germanium etching using time multiplexed plasma etching, J. Vac. Sci. Technol. B 33 (2015) 060605. URL: https://doi.org/10.1116/1.4936112, https://doi.org/10.1116/1.4936112. arXiv:https://doi.org/10.1116/1.4936112.

[10] M. de Lafontaine, M. Darnon, C. Colin, B. Bouzazi, M. Volatier, R. Arès, S. Fafard, V. Aimez, A. Jaouad, Impact of via hole integration on multijunction solar cells for through cell via contacts and associated passivation treatment, IEEE J. Photovoltaics 7 (2017) 1456–1461.

[11] M. de Lafontaine, E. Pargon, C. Petit-Etienne, G. Gay, A. Jaouad, M.J. Gour, M. Volatier, S. Fafard, V. Aimez, M. Darnon, Influence of plasma process on iii-v/ge multijunction solar cell via etching, Sol. Energy Mater. Sol. Cells 195 (2019) 49–54. URL: http://www.sciencedirect.com/science/article/pii/S0927024819300418, https://doi.org/10.1016/j.solmat.2019.01.048.

[12] L. Desvoivres, L. Vallier, O. Joubert, X-ray photoelectron spectroscopy investigation of sidewall passivation films formed during gate etch processes, J. Vacu. Sci. Technol B: Microelectr. Nanometer Struct. Proces. Measure. Phenomena 19 (2001) 420–426. URL: https://avs.scitation.org/doi/abs/10.1116/1.1352727, https://doi.org/10.1116/1.1352727. arXiv:https://avs.scitation.org/doi/pdf/10.1116/1.1352727.

[13] F. Dimroth, M. Grave, P. Beutel, U. Fiedeler, C. Karcher, T.N.D. Tibbits, E. Oliva, G. Siefer, M. Schachtner, A. Wekkeli, A.W. Bett, R. Krause, M. Piccin, N. Blanc, C. Drazek, E. Guiot, B. Ghyselen, T. Salvetat, A. Tauzin, T. Signamarcheix, A. Dobrich, T. Hannappel, K. Schwarzburg, Wafer bonded four-junction gainp/gaas//gainasp/gainas concentrator solar cells with 44.7% efficiency, Prog. Photovolt. Res. Appl. 22 (2014) 277–282. URL: https://onlinelibrary.wiley.com/doi/abs/10.1002/pip.2475, https://doi.org/10.1002/pip.2475. arXiv:https://onlinelibrary.wiley.com/doi/pdf/10.1002/pip.2475.

[14] P. Espinet-González, I. Rey-Stolle, M. Ochoa, C. Algora, I. García, E. Barrigón, Analysis of perimeter recombination in the subcells of gainp/gaas/ge triple-junction solar cells, Prog. Photovolt. Res. Appl. 23 (2015) 874–882. URL: https://onlinelibrary.wiley.com/doi/abs/10.1002/pip.2501, https://doi.org/10.1002/pip.2501. arXiv:https://onlinelibrary.wiley.com/doi/pdf/10.1002/pip.2501.

[15] Fafard, S., 2001. Solar cell with epitaxially grown quantum dot material. URL: https://patents.google.com/patent/US7863516B2/ko. u.S. Patent No. 7,863,516.

[16] L. Gatilova, S. Bouchoule, S. Guilet, P. Chabert, Investigation of inp etching mechanisms in a cl2/h2 inductively coupled plasma by optical emission spectroscopy, J. Vac. Sci. Technol. A 27 (2009) 262–275. URL: https://doi.org/10.1116/1.3071950, https://doi.org/10.1116/1.3071950. arXiv:https://doi.org/10.1116/1.3071950.

[17] J. Geisz, R. France, K. Schulte, M. Steiner, A. Norman, H. Guthrey, M. Young, T. Song, T. Moriarty, Six-junction iii–v solar cells with 47.1% conversion efficiency under 143 suns concentration, Nat. Energy 5 (2020), https://doi.org/10.1038/s41560-020-0598-5.

[18] R.A. Gottscho, B.L. Preppernau, S.J. Pearton, A.B. Emerson, K.P. Giapis, Real-time monitoring of low-temperature hydrogen plasma passivation of gaas, J. Appl. Phys. 68 (1990) 440–445. URL: https://doi.org/10.1063/1.346813, https://doi.org/10.1063/1.346813. arXiv:https://doi.org/10.1063/1.346813.

[19] S. Guilet, S. Bouchoule, C. Jany, C.S. Corr, P. Chabert, Optimization of a cl2–h2 inductively coupled plasma etching process adapted to nonthermalized inp wafers for the realization of deep ridge heterostructures, J. Vacu. Sci. Technol B: Microelectr. Nanometer Struct. Proces. Measure. Phenomena 24 (2006) 2381–2387, https://doi.org/10.1116/1.2348728.

[20] R. Huang, X.Y. Lin, Y.P. Yu, K.X. Lin, J.H. Wei, C.Y. Yu, Z.K. Wang, Fast growth of polycrystalline film in sicl4/h2 plasma, Chin. Phys. Lett. 21 (2004) 1168–1170, https://doi.org/10.1088/0256-307X/21/6/053.

[21] H. Hubner, Calculations on deposition and redeposition in plasma etch processes, J. Electrochem. Soc. 139 (1992) 3302–3309. URL: https://doi.org/10.1149%2F1.2069072, https://doi.org/10.1149/1.2069072.

[22] N.M. Johnson, R.D. Burnham, R.A. Street, R.L. Thornton, Hydrogen passivation of shallow-acceptor impurities in p-type gaas, Phys. Rev. B 33 (1986) 1102–1105. URL: https://link.aps.org/doi/10.1103/PhysRevB.33.1102, https://doi.org/10.1103/PhysRevB.33.1102.

[23] M. Lafontaine, A. Jaouad, M. Darnon, M. Volatier, R. Arès, S. Fafard, V. Aimez, Via sidewall insulation for through cell via contacts, 2017, p. 040002, https://doi.org/10.1063/1.5001424.

[24] J. Lagowski, M. Kaminska, J.M. Parsey, H.C. Gatos, M. Lichtensteiger, Passivation of the dominant deep level (el2) in gaas by hydrogen, Appl. Phys. Lett. 41 (1982) 1078–1080. URL: https://doi.org/10.1063/1.93407, https://doi.org/10.1063/1.93407. arXiv:https://doi.org/10.1063/1.93407.

[25] J. Landesman, C. Levallois, J. Jiménez, F. Pommereau, Y. Léger, A. Beck, T. Delhaye, A. Torres, C. Frigeri, A. Rhallabi, Evidence of chlorine ion penetration in inp/inasp quantum well structures during dry etching processes and effects of induced-defects on the electronic and structural behaviour, Microelectron. Reliab. 55 (2015) 1750–1753. URL: http://www.sciencedirect.com/science/article/pii/S0026271415301153, https://doi.org/10.1016/j.microrel.2015.07.029. proceedings of the 26th European Symposium on Reliability of Electron Devices, Failure Physics and Analysis.

[26] O. Luere, E. Pargon, L. Vallier, B. Pelissier, O. Joubert, Etch mechanisms of silicon gate structures patterned in sf6/ch2f2/ar inductively coupled plasmas, J. Vac. Sci. Technol. B 29 (2011) 011028. URL: https://doi.org/10.1116/1.3522656, doi: 10.1116/1.3522656, arXiv:https://doi.org/10.1116/1.3522656.

[27] D. Ohori, T. Fujii, S. Noda, W. Mizubayashi, K. Endo, E.T. Lee, Y. Li, Y.J. Lee, T. Ozaki, S. Samukawa, Atomic layer germanium etching for 3d fin-fet using chlorine neutral beam, J. Vac. Sci. Technol. A 37 (2019), 021003, https://doi.org/10.1116/1.5079692.

[28] E. Oliva, T. Salvetat, C. Jany, R. Thibon, H. Helmers, M. Steiner, M. Schachtner, P. Beutel, V. Klinger, J.S. Moulet, F. Dimroth, Iii-V Multi-Junction Metal-Wrap-through (Mwt) Concentrator Solar Cells, 2016, https://doi.org/10.4229/EUPVSEC20162016-4CO.6.1.

[29] S.J. Pearton, C.R. Abernathy, R.F. Kopf, F. Ren, Low temperature chlorine-based dry etching of III–v semiconductors, J. Electrochem. Soc. 141 (1994) 2250–2256. URL: https://doi.org/10.1149%2F1.2055098, https://doi.org/10.1149/1.2055098.

[30] V. Renaud, C. Petit-Etienne, J.P. Barnes, J. Bisserier, O. Joubert, E. Pargon, Two-step cycling process alternating implantation and remote plasma etching for topographically selective etching: application to si3n4 spacer etching, J. Appl. Phys. 126 (2019) 243301. URL: https://doi.org/10.1063/1.5131030, doi: 10.1063/1.5131030, arXiv:https://doi.org/10.1063/1.5131030.

[31] O. Richard, V. Aimez, R. Arès, S. Fafard, A. Jaouad, Simulation of through-cell vias contacts under non-uniform concentrated light profiles, Sol. Energy Mater. Sol. Cells 188 (2018) 241–248. URL, http://www.sciencedirect.com/science/article/pii/S0927024818304379, https://doi.org/10.1016/j.solmat.2018.08.023.

[32] O. Richard, S. Blais, R. Arès, V. Aimez, A. Jaouad, Mechanisms of gaas surface passivation by a one-step dry process using low-frequency plasma enhanced chemical deposition of silicon nitride, Microelectron. Eng. 233 (2020) 111398. URL: http://www.sciencedirect.com/science/article/pii/S0167931720301866, https://doi.org/10.1016/j.mee.2020.111398.

[33] O. Richard, A. Jaouad, B. Bouzazi, R. Arès, S. Fafard, V. Aimez, Simulation of a through cell via contacts architecture for hcpv multi-junction solar cells, Sol. Energy Mater. Sol. Cells 144 (2016) 173–180. URL, http://www.sciencedirect.com/science/article/pii/S0927024815004262, https://doi.org/10.1016/j.solmat.2015.08.032.

[34] T. Salvetat, E. Oliva, A. Tauzin, V. Klinger, P. Beutel, C. Jany, R. Thibon, P. H. Haumesser, A. Hassaine, T. Mourier, G. Rodriguez, C. Lecouvey, B. Imbert, F. Fournel, J.M. Fabbri, J.S. Moulet, F. Dimroth, T. Signamarcheix, M. Wiesenfarth, A. Bett, M. Muller, Iii-v multi-junction solar cell using metal wrap through contacts, AIP Conference Proceedings 1766 (2016) 060004. URL: https://aip.scitation.org/doi/abs/10.1063/1.4962094, doi: 10.1063/1.4962094, arXiv:https://aip.scitation.org/doi/pdf/10.1063/1.4962094.

[35] T. Soga, T. Jimbo, G. Wang, K. Ohtsuka, M. Umeno, Hydrogen plasma passivation of gaas on si substrates for solar cell fabrication, J. Appl. Phys. 87 (2000) 2285–2288. URL: https://doi.org/10.1063/1.372174, https://doi.org/10.1063/1.372174. arXiv:https://doi.org/10.1063/1.372174.

[36] G. Wang, T. Ogawa, T. Soga, T. Jimbo, M. Umeno, A detailed study of h2 plasma passivation effects on gaas/si solar cell, Sol. Energy Mater. Sol. Cells 66 (2001) 599–605. URL, http://www.sciencedirect.com/science/article/pii/S0927024800002452, https://doi.org/10.1016/S0927-0248(00)00245-2. pVSEC 11 - Part II.

[37] Y. Zhao, P. Fay, A. Wibowo, J. Liu, C. Youtsey, Via-hole fabrication for iii-v triple-junction solar cells, J. Vacu. Sci. Technol B: Microelectr. Nanometer Struct. 30 (2012), https://doi.org/10.1116/1.4754306.

[38] Y. Zhao, P. Fay, A. Wibowo, C. Youtsey, Inductively coupled plasma etching of through-cell vias in iii–v multijunction solar cells using sicl4/ar, J. Vac. Sci. Technol. B 31 (2013), https://doi.org/10.1116/1.4822015, 06FF05. URL: https://doi.org/10.1116/1.4822015. arXiv:https://doi.org/10.1116/1.4822015.